YMTHE, Volume *29*

Supplemental Information

The CD39^{+} HBV surface protein-targeted CAR-T and personalized tumor-reactive CD8^{+} T cells exhibit potent anti-HCC activity

Fan Zou, Jizhou Tan, Ting Liu, Bingfeng Liu, Yaping Tang, Hui Zhang, and Jiaping Li

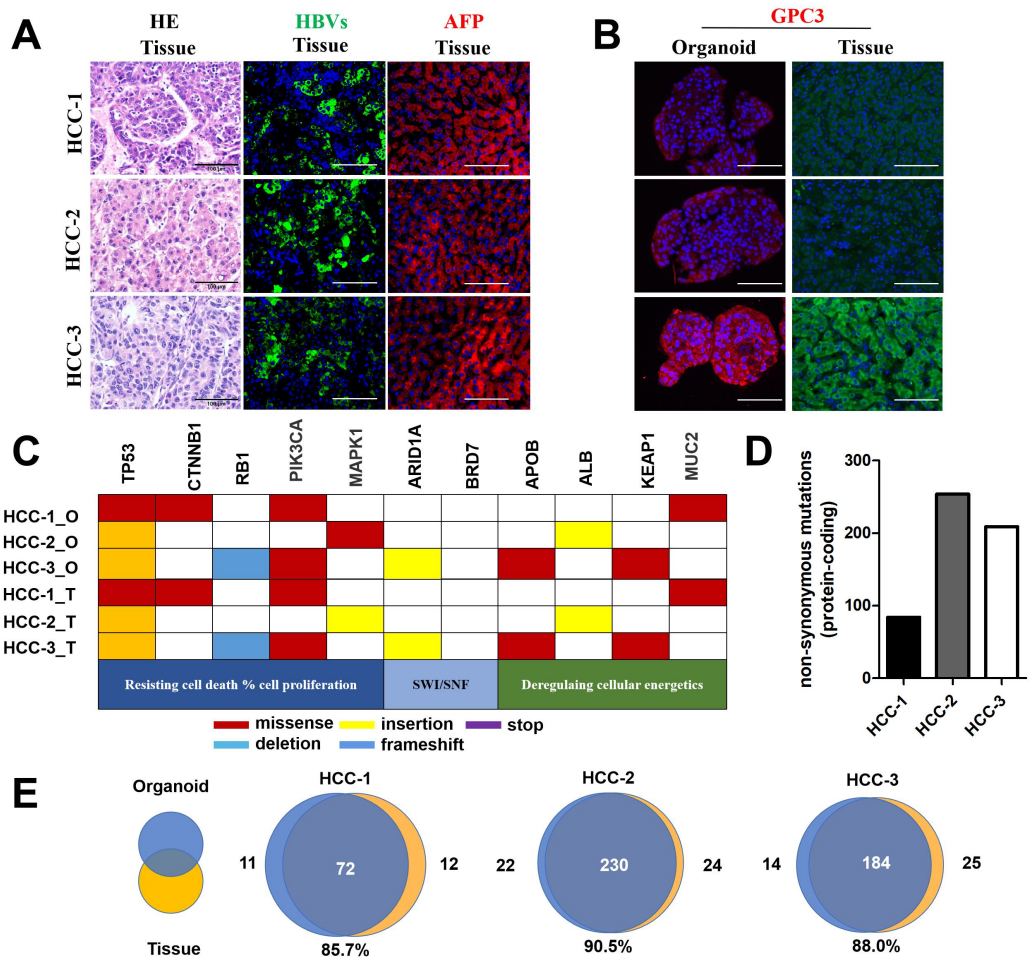

Supplementary Figure 1. Immunofluorescent images and repertoire of genetic characteristics in the HCC originating tissues and their organoids.

(A). Immunofluorescent analysis was used to show the expression of AFP, HBVs protein on HCC tissue of three patients.

(B). Immunofluorescent analysis was used to show the expression of GPC-3 on HCC tissue and organoids of three patients.

(C). Tumor mutation burden of non-synonymous mutations of the three patients was shown.

(D). Repertoire of somatic non-synonymous mutation status of genes significantly mutated in HCC according to cWES. Mutation types are indicated in different colors.

(E). Venn diagrams illustrate the number of somatic non-synonymous mutations present in each HCC tissues and HCC organoids.

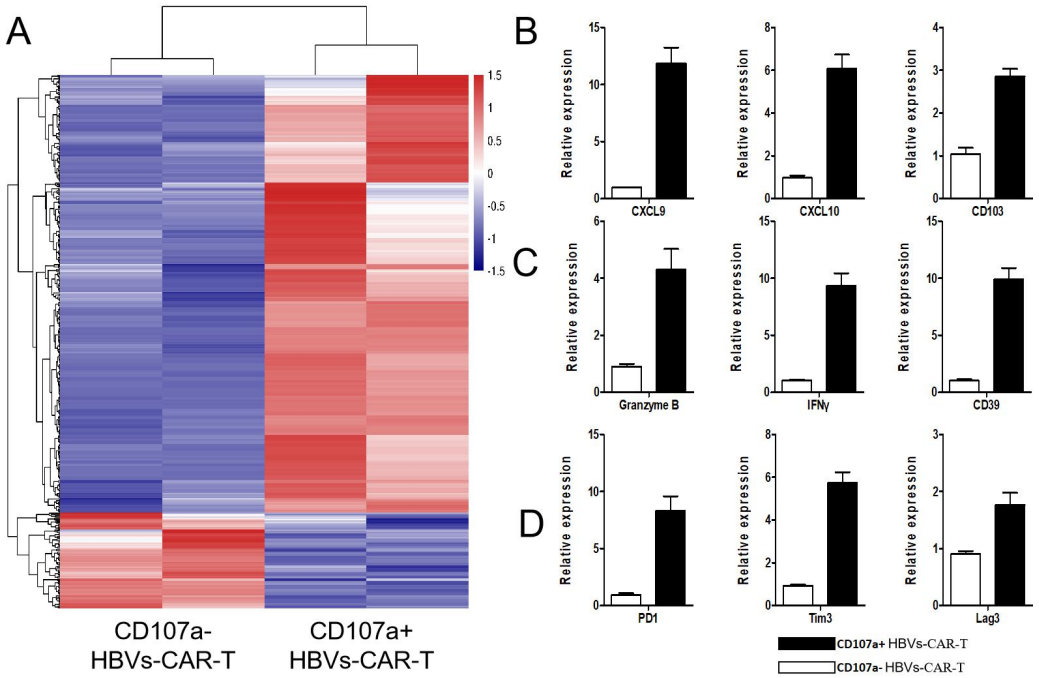

Supplementary Figure 2. Gene expression of CD107a-positive effector HBVs-CAR-T cells.

(A). CAR-T cells were obtained by FACS sorting after co-culture with the E:T ratio of 10:1 for 24 hours. Heatmap of RNA-sequence showed the expression of genes with P-value < 0.01. RNA expression levels were respectively indicated with a red/blue scale for high and low expression levels.

(B-D). qRT-PCR revealed the relative mRNA expression level of genes in $CD107a^{+}$/$CD107a^{-}$ HBVs-CAR-T cells respectively.

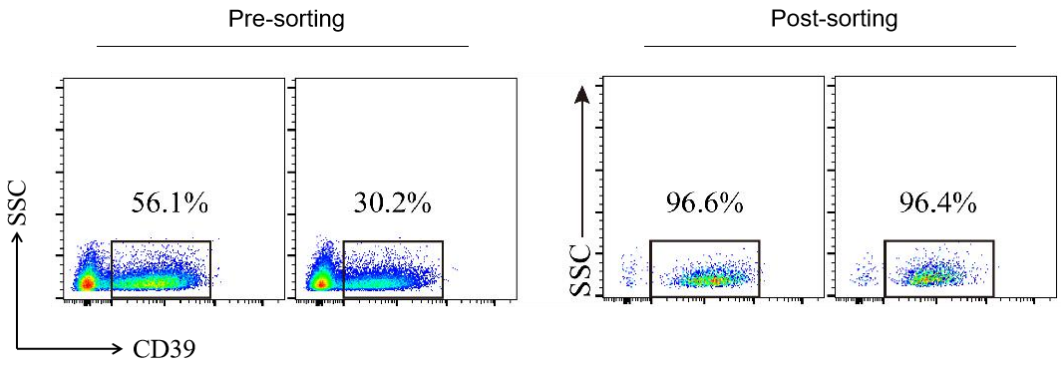

Supplementary Figure 3. Sorting efficacy of CD39⁺ HBVs-CAR T cells by flow sorting.

Sorting efficacy of CD39⁺ HBVs-CAR T cells by FACS could achieve over 95%.

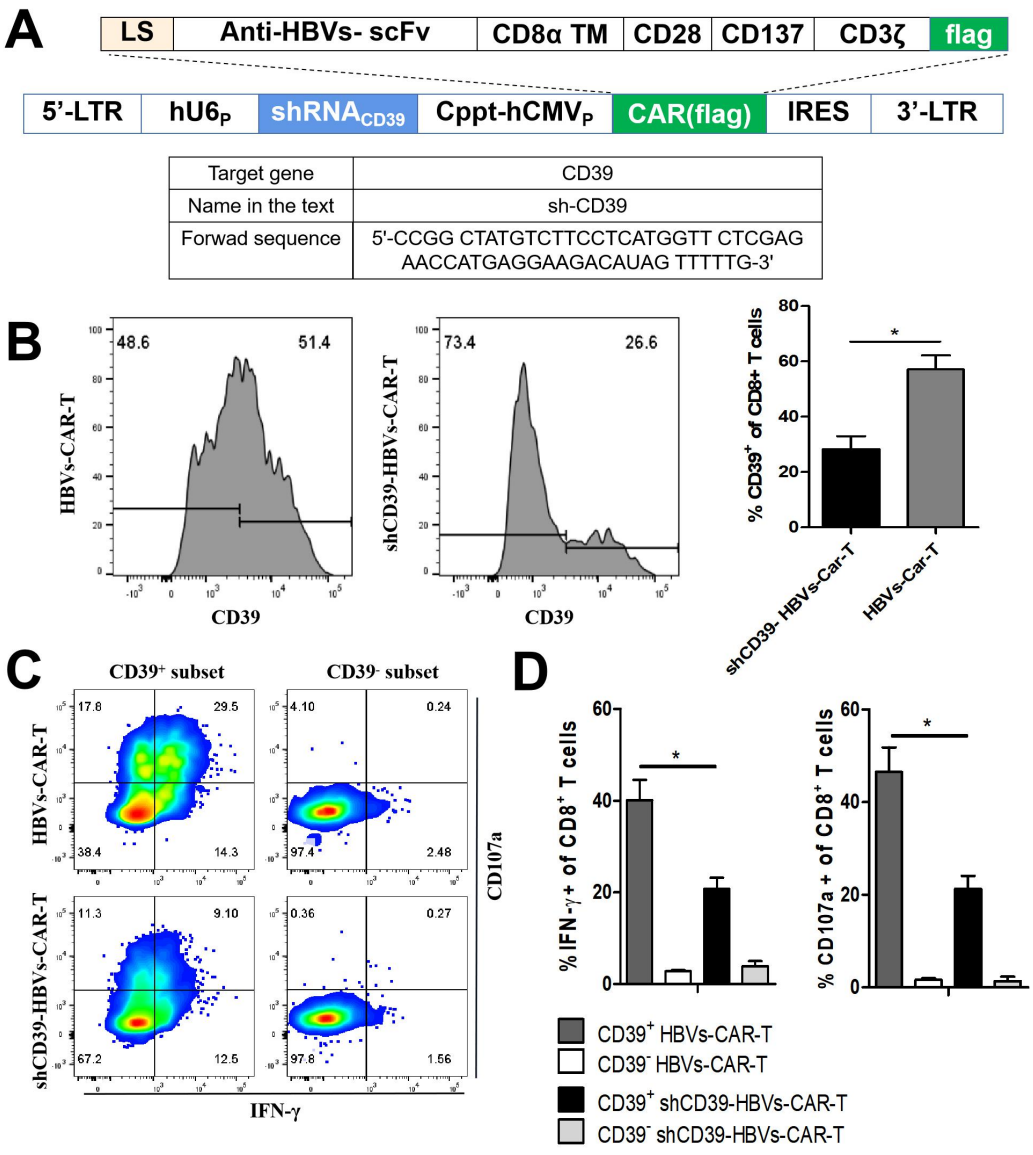

Supplementary Figure 4. Knock-down CD39 on HBVs-CAR-T cells resulted in a decreased cytotoxic T lymphocyte activity.

(A) . Schematic representation of the lentiviral vectors carrying a HBVs-specific CAR moiety and a cluster of sh-CD39.

(B) . Flow cytometry revealed the knock-down efficiency of CD39 on HBVs-CAR-T cells.

(C-D). Relative quantification of IFN-γ production and CD107a expression in $CD39^{+}/CD39^{-}CD8^{+}$ HBVs-CAR-T and shCD39-HBVs-CAR-T cells. Error bars represent SEM of three biological replicates.

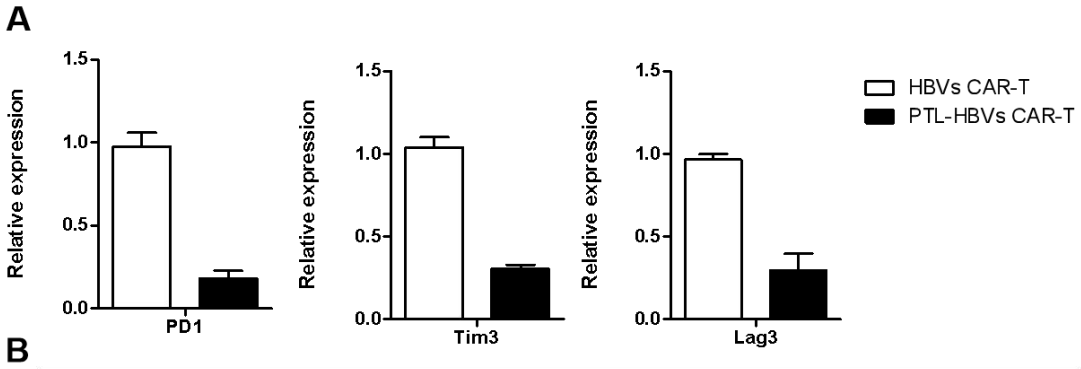

B

Target gene	Name in the text	Target sequence
PD-1	sh-PD-1	GCTTCGTGCTAAACTGGTA
Tim-3	sh-Tim-3	ACTCTAGATTGGCCAATGA
Lag-3	sh-Lag-3	TGGCGACTTTACCCTTCGA

Supplementary Figure 5. HBVs-specific CAR-T cells carrying various co-receptor-specific shRNAs.

(A). Relative mRNA expression level of inhibitory receptors in HBVs-CAR-T cells with down-regulation of PD-1, Lag-3, or Tim-3 respectively (14 days post infection) (n = 3, 3 healthy donors).

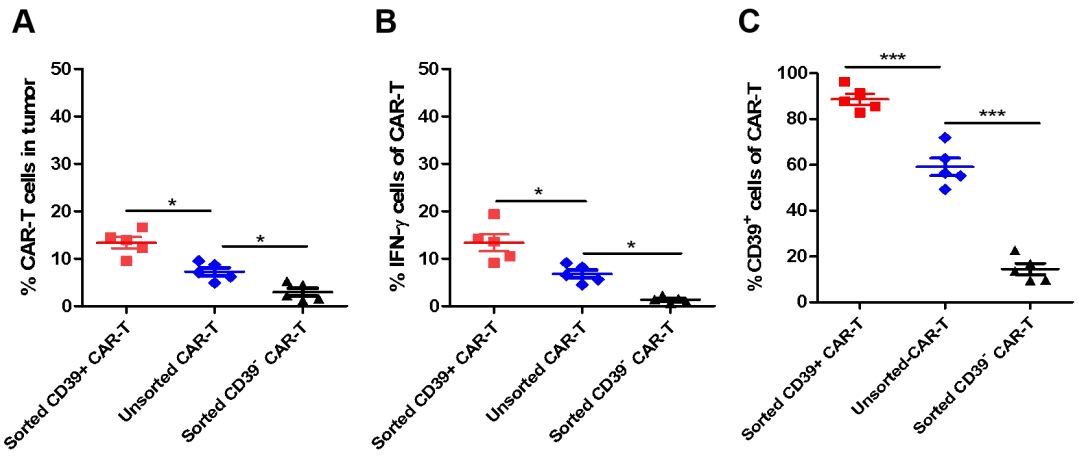

43

44 **Supplementary Figure 6. Sorted CD39^{+} HBVs-CAR-T exerted stronger**

45 **cytotoxicity than unsorted HBVs-CAR-T in vivo.**

46 HBVs-CAR-T cells were generated as previously described, and divided into sorted

47 CD39$^{+/-}$ groups and unsorted group. T cells was adoptive transfered into NSG mice

48 with HCC PDX model. Each mouse was injected 1×10^{6} T cells(sorted CD39^{+}, sorted

49 CD39^{-}, and unsorted CAR-T) via a single intravenous (i.v.) injection. On day 14,

50 tumor tissues were collected and digested. Tumor infiltrating T cells were tested by

51 Flow cytometry.

52 (A) . Flow cytometry revealed the frequency of infiltrating CAR-T cells.

53 (B-C). The frequency of IFN-γ positive and CD39 positive in CAR-T cells were

54 shown.